4. J. D. Luttmer and A. J. Bard, *This Journal*, **125**, 1424 (1978).
5. H. H. Strickert, J. R. Tong, and A. B. Ellis, *J. Am. Chem. Soc.*, **104**, 581 (1982).
6. Y. Nakato, H. Ogawa, K. Morita, and H. Tsubomura, *J. Phys. Chem.*, **90**, 6210 (1986).
7. G. Nogami and Y. Nishiyama, *This Journal*, **135**, 3038 (1988).
8. R. V. Kasowski and R. H. Tait, *Phys. Rev.*, **B20**, 5168 (1979).
9. R. Wilson, *J. Appl. Phys.*, **48**, 4292 (1977).
10. G. Nogami, Y. Ogawa, and Y. Nishiyama, *This Journal*, **135**, 3008 (1988).
11. P. Salvador, *ibid.*, **128**, 1895 (1981).
12. F.-R. F. Fan and A. J. Bard, *J. Phys. Chem.*, **94**, 3761 (1990).

A Graphical Ellipsometric Data Reduction Algorithm and Its Application in Thin SiO_2 Film Measurement

H. F. Wei and A. K. Henning

Thayer School of Engineering, Dartmouth College, Hanover, New Hampshire 03755

J. Slinkman

IBM General Technology Division, Essex Junction, Vermont 05452-4299

W. R. Hunter

SFA, Incorporated, Landover, Maryland 20785

ABSTRACT

Graphical ellipsometric data reduction algorithm, based on independent analysis of both the real and imaginary parts of the ellipsometry equation, is described and compared with other established algorithms in terms of both one- and two-layer nonabsorbing film models. Issues relating to thin SiO_2 film measurement are discussed, using the graphical ellipsometric data reduction algorithm. Some intrinsic properties of the ellipsometry equation, which are of practical importance, are presented for the first time using the proposed algorithm, previously impossible with other ellipsometric data reduction algorithms. In particular, it is found the imaginary part of the ellipsometry equation has considerable resistance to common measurement errors encountered in thin SiO_2 film measurement. All phenomena presented are based on a nonabsorbing one-layer SiO_2 film model. Similar phenomena may also be observed in the case of a nonabsorbing, two-layer SiO_2 model. The special case of an absorbing one-layer film model is also examined.

For measuring thin oxide films (less than 200 Å) using ellipsometry in a production environment, it is often necessary to fix the refractive index in order to obtain oxide thickness. That refractive index and oxide thickness cannot be extracted simultaneously with data reduction software associated with ellipsometers may be due to either the poor convergence of the data reduction algorithm (1), or ellipsometer measurement errors, or both. This calls for a reliable ellipsometric data reduction algorithm which is capable of monitoring the unknown extraction process, distinguishing between the sources of the problem just mentioned, simulating the impact of measurement errors on data reductions, and offering compensation to the final solutions. We present the following graphical ellipsometric data reduction algorithm which fulfills these requirements. The algorithm is general enough to handle cases common in thin-film measurement (*e.g.*, absorbing films or a multi-layer film system), though only two unknowns are allowed.

Experiment Details

Samples No. 1 and No. 2 used in this study are device-quality boron-doped (resistivity $11 \sim 16\ \Omega \cdot cm$) <100> 5 in. silicon wafers. They received a standard RCA clean and were then oxidized in dry O_2 at 800°C at the IBM General Technology Division facility in Essex Junction, Vermont. Sample No. 3 is a bare <100> silicon wafer (with natural oxide). The Rudolph Research Model 436 manual ellipsometer at the Measurement Standards Lab of IBM GTD Essex Junction was used as the primary ellipsometer, and has polarizer and analyzer resolutions of 0.01° (2). The Gaertner Scientific ellipsometer L104SA at Dartmouth was used for comparison. The Gaertner ellipsometer is a rotating analyzer ellipsometer with a resolution of around 0.1° as indicated on the polarizer and analyzer scale. Both ellipsometers were operated at a wavelength of 6328 Å.

Numerical Procedure

Essentially there are three ellipsometric data reduction algorithms in the literature: the conventional iterating algorithm to search for the solution of the thickness until its imaginary part vanishes, the least-squares Δ and ψ error term analysis algorithm (3), and the algorithm based on the combination of random search and *regula falsi* procedures to minimize the Δ and ψ error radius (1).

The algorithm of this study traces both the real and imaginary parts of the ellipsometry equation in the plane of the two unknowns (refractive index and film thickness for the case of a one-layer model), then seeks their intersection in this plane. The ellipsometry equation is expressed as (4)

$$\tan(\psi) \exp(i\Delta) = R_p/R_s \quad [1]$$

where Δ and ψ describe the state of polarization of reflected light, and R_p and R_s are the total Fresnel reflection coefficients at the film surface for p- and s-polarized monochromatic light. The particular expressions for R_p and R_s are film-model-dependent (*e.g.*, one- or two-layer model, models incorporating stress-optic effect or optical anisotropy) (4). The equations leading to the final expressions of R_p and R_s are as follows for the one-layer model (5)

$$r_{s,i} = \frac{N_{i-1} \cos \theta_{i-1} - N_i \cos \theta_i}{N_{i-1} \cos \theta_{i-1} + N_i \cos \theta_i} \quad [2]$$

$$r_{p,i} = \frac{N_i \cos \theta_{i-1} - N_{i-1} \cos \theta_i}{N_i \cos \theta_{i-1} + N_{i-1} \cos \theta_i} \quad [3]$$

$$\alpha = \frac{4\pi d}{\lambda}\sqrt{N_1^2 - N_0^2 \sin^2\theta_0} \quad [4]$$

$$N_0 \sin\theta_0 = N_1 \sin\theta_1 = N_2 \sin\theta_2 \quad [5]$$

$$R_s = \frac{r_{s,1} + r_{s,2}\cdot e^{-i\alpha}}{1 + r_{s,1}\cdot r_{s,2}\cdot e^{-i\alpha}} \quad [6]$$

$$R_p = \frac{r_{p,1} + r_{p,2}\cdot e^{-i\alpha}}{1 + r_{p,1}\cdot r_{p,2}\cdot e^{-i\alpha}} \quad [7]$$

where $r_{s,i}$ and $r_{p,i}$ are the Fresnel reflection coefficients at the i-th interface for s- and p-polarized light (the ambient-to-film interface corresponds to $i = 1$; the film-to-substrate interface corresponds to $i = 2$); N_0, N_1, and N_2 are complex refractive indexes for the ambient (air), film, and the substrate ($N = n - ik$, where n is the index of refraction [the real part of N] and k is the extinction coefficient [the imaginary part of N]; θ_0 is the angle of incidence at the first interface (ambient/film), θ_1 and θ_2 are angles of refraction; α is the phase factor in the film for s- or p-polarized light; R_p and R_s are the total Fresnel reflection coefficients for p- and s-polarized light. Equation [5] is Snell's law (law of refraction).

Since Δ and ψ can be measured by an ellipsometer, Eq. [1] can be viewed as containing only two unknowns (specifically, film thickness d and film index of refraction n_1 for the case of the one-layer model), provided all other variables in Eq. [2] to [7] are known. The algorithm we present uses a unique method to solve Eq. [1] for the two unknowns: instead of using one of the three established methods mentioned in the beginning of this section, our algorithm simply displays Eq. [1] numerically on the two-unknown plane of physical significance (the $d - n_1$ plane for a one-layer model). In other words, on a predetermined two-unknown plane which may contain the physical solution of the two unknowns (d and n_1), our algorithm seeks every pair of numerical values of the two unknowns which balance either the real or the imaginary part of Eq. [1]. Thus two curves can be located or traced on the plane: the real one and the imaginary one. Obviously the physical solution to Eq. [1] is the intersection of the real curve and the imaginary curve. In later sections it can be seen that it is this unique method in solving Eq. [1] which reveals the intrinsic properties of the ellipsometry equation, previously not found by other ellipsometry equation solvers.

The curve tracing procedure used in this study is different than that used in isoreflectance curve tracing (6). For simplicity, we describe only the procedure to trace the real curve of Eq. [1]. The imaginary curve tracing is done similarly. The procedure to trace one curve is illustrated in Fig. 1. Starting with a given window (which preferably has physical meaning in order to minimize searching effort) in the two-unknown plane, where all other variables of the ellipsometry equation are known or assumed, the program locates the first solution point of the real part of Eq. [1] (the pair of numerical values of the two unknowns which can

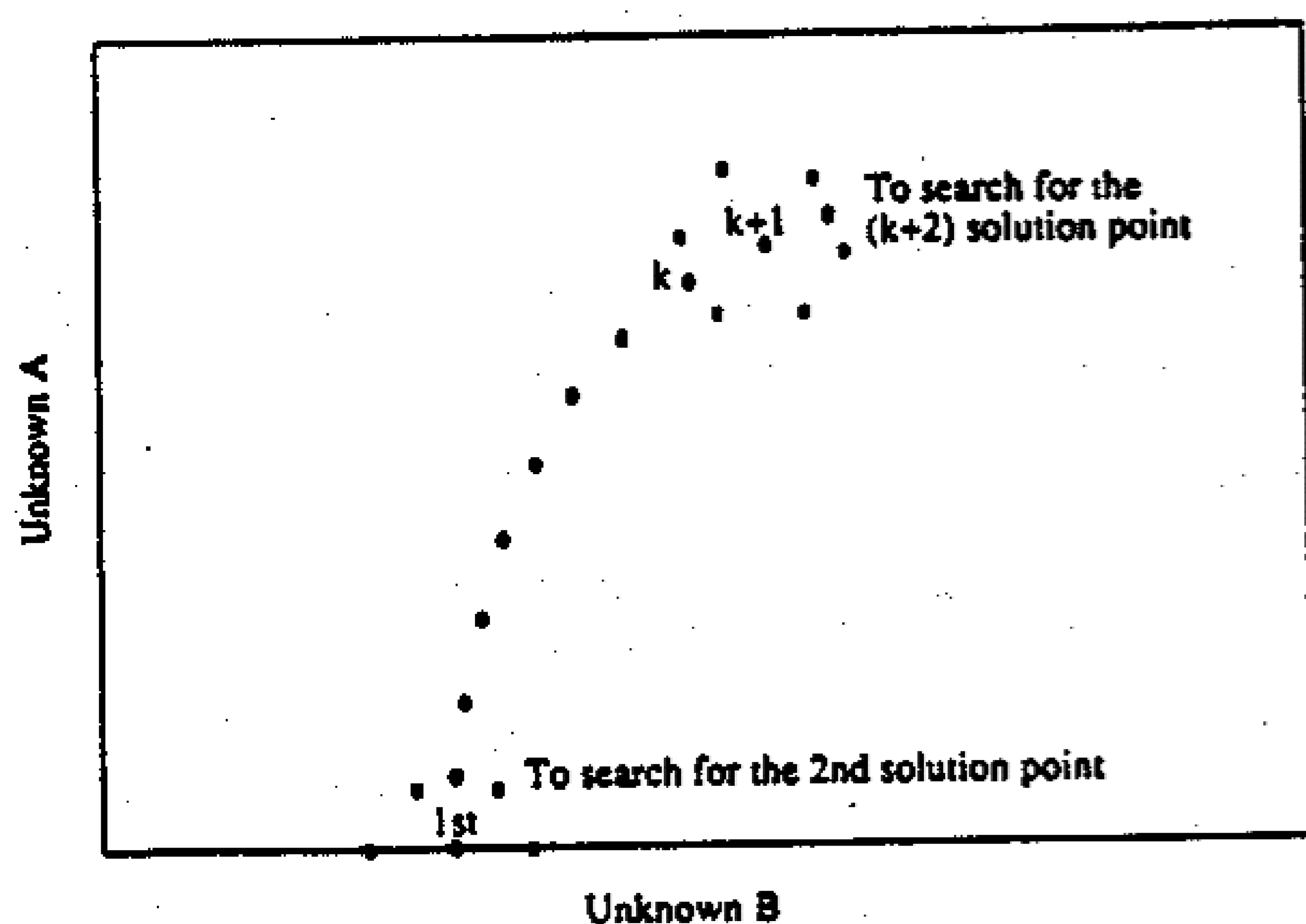

Fig. 1. Tracing the real part of the ellipsometry equation on the two-unknown planes.

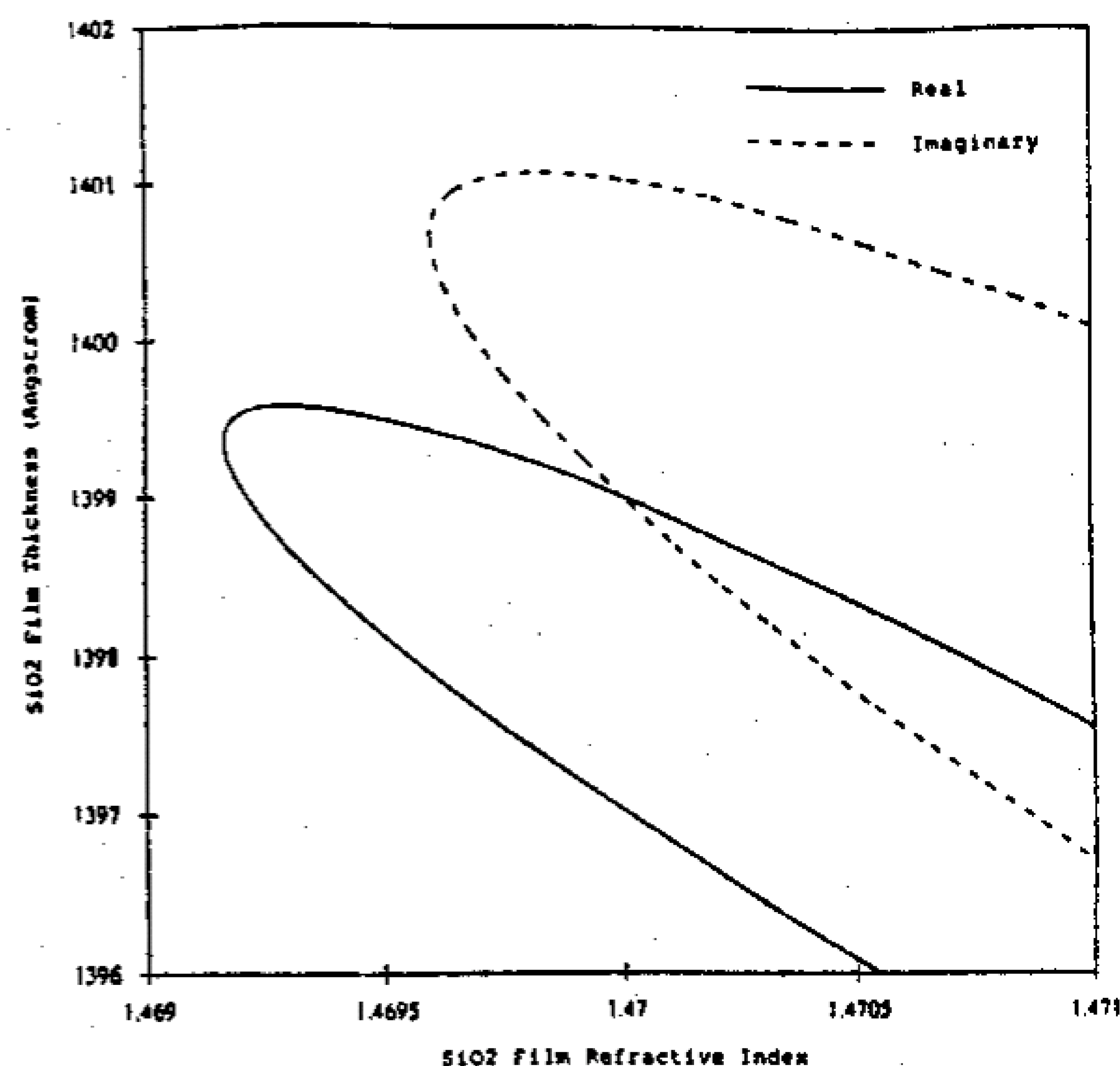

Fig. 2. Multivalue nature of ellipsometric real and imaginary curves for 1399 Å thick SiO_2 film with refractive index of 1.47 (one-layer model SiO_2 on Si).

balance the real part of Eq. [1] in the selected window using the bisection method. The program then generates a circle centered at the first solution point with a radius of the chosen searching step-size. Six symmetry locations on the circle are generated, dividing the circle into equal arcs. To obtain the second solution point for the real part of the ellipsometry equation, the angle bisection method is used on the arc (inside the window) for which the function studied has opposite signs at the ends of the arc.

If the solution point is already inside the window (*e.g.*, the point $(k + 1)$ in Fig. 1), to search for the point $(k + 2)$ arcs containing the solution point k are not considered, to prevent curve tracing back. It is rare that the curve being traced has a tangent angle sharper than 30°. If necessary, the number of arc-dividing locations generated on the circle can be increased to more than six. The tracing continues until the solution point is out of the selected window. If the bisection method is not applicable during the searching procedure, the program will stop to ask for a finer searching step-size.

After both real and imaginary curves are traced, their intersection in the two-unknown plane is taken to be the physical solution to Eq. [1], even if this intersection is outside the selected window. Notice the precision of this physical solution is limited by the searching step size and by the stopping criterion used in the bisection routine. For some special cases there can be more than one curve for the real or imaginary part within a chosen window. Multiple intersections of the real and imaginary curves within a physical region (*i.e.*, refractive index larger than unity and film thickness within the first ellipsometric cycle) have never been observed in this study.

Compared with a direct root solver which locates the curves studied on the mesh of the two-unknown plane,

Table I. Calculated Δ and ψ values from hypothetical film thickness d and refractive index n of the one-layer model with AOI = 70°, WVL = 6328 Å, (100) silicon substrate with n-Si = 3.8737 and k-Si = 0.018, n-air = 1.0, using the algorithm of this study and single precision FORTRAN.

Δ	ψ	Thickness (Å)	n
165.7669830	10.70663929	40	1.77
163.1347809	10.80327320	50	1.65
160.4936523	10.91312695	60	1.60
157.5273132	11.04862785	70	1.60
154.6274414	11.20185471	80	1.60
149.0462189	11.55789471	100	1.60
137.6553040	12.61900711	150	1.55
78.66716766	41.77760696	1000	1.47

Table II. Solutions of the film thickness and refractive index given by this algorithm and Gaertner program using the calculated Δ and ψ values of Table I (thickness rounded off to integer and refractive index rounded off to the third digit after the decimal).

Algorithm of this study (Using untruncated Δ and ψ data)		Gaertner program		Algorithm of this study (Truncated Δ and ψ data to third digit after decimal)		Gaertner program	
Thickness (Å)	n	Thickness (Å)	n	Thickness (Å)	n	Thickness (Å)	n
40	1.770	40	1.770	40	1.766	40	1.766
50	1.650	50	1.650	50	1.652	50	1.652
60	1.600	60	1.600	60	1.601	60	1.601
70	1.600	70	1.600	70	1.599	70	1.598
80	1.600	80	1.600	80	1.600	80	1.600
100	1.600	100	1.600	100	1.600	100	1.600
150	1.550	150	1.550	150	1.550	150	1.550
1000	1.470	1000	1.470	1000	1.470	1000	1.470

this tracing method is computationally more efficient, since it only searches the vicinity of the curves. Figure 2 illustrates a solution graph using the state of polarization calculated from 1399 Å thick SiO_2 film (n-SiO_2 = 1.47) with n − air = 1.0, angle of incidence (AOI) = 70°, and wavelength = 6328 Å. Since multiple values of the real and imaginary parts are possible even within a very narrow physical region as shown in Fig. 2, this tracing method demonstrates its efficiency over direct multiroot solvers which usually require knowledge of the first derivative of the ellipsometric function studied.

Comparison and Evaluation of Ellipsometric Data Reduction Algorithms: Software vs. Hardware

The graphical ellipsometric data reduction algorithm was implemented on the IBM RS6000 in FORTRAN. In most cases it takes a few seconds to complete one run, yielding the physical solution to the ellipsometry equation

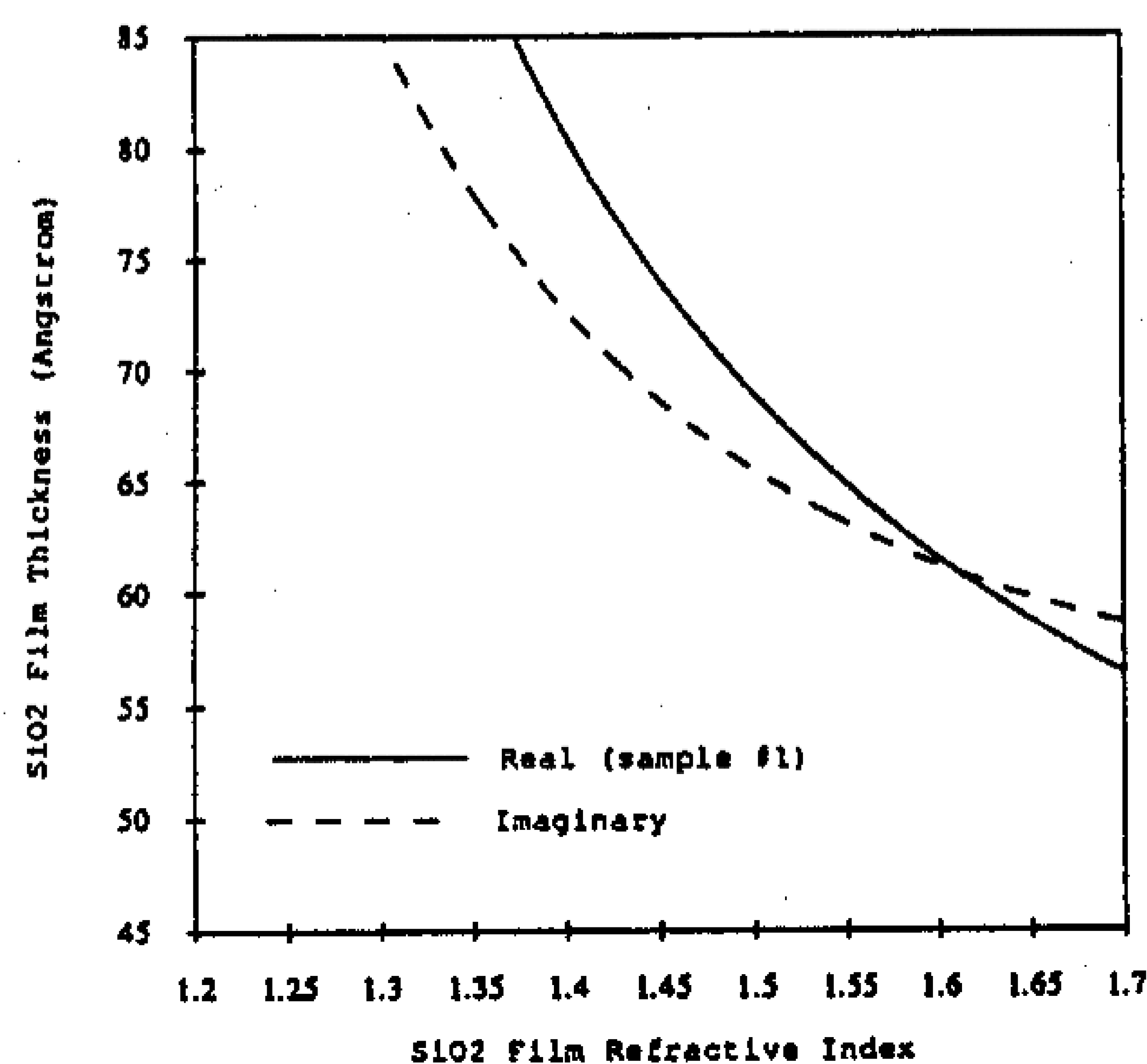

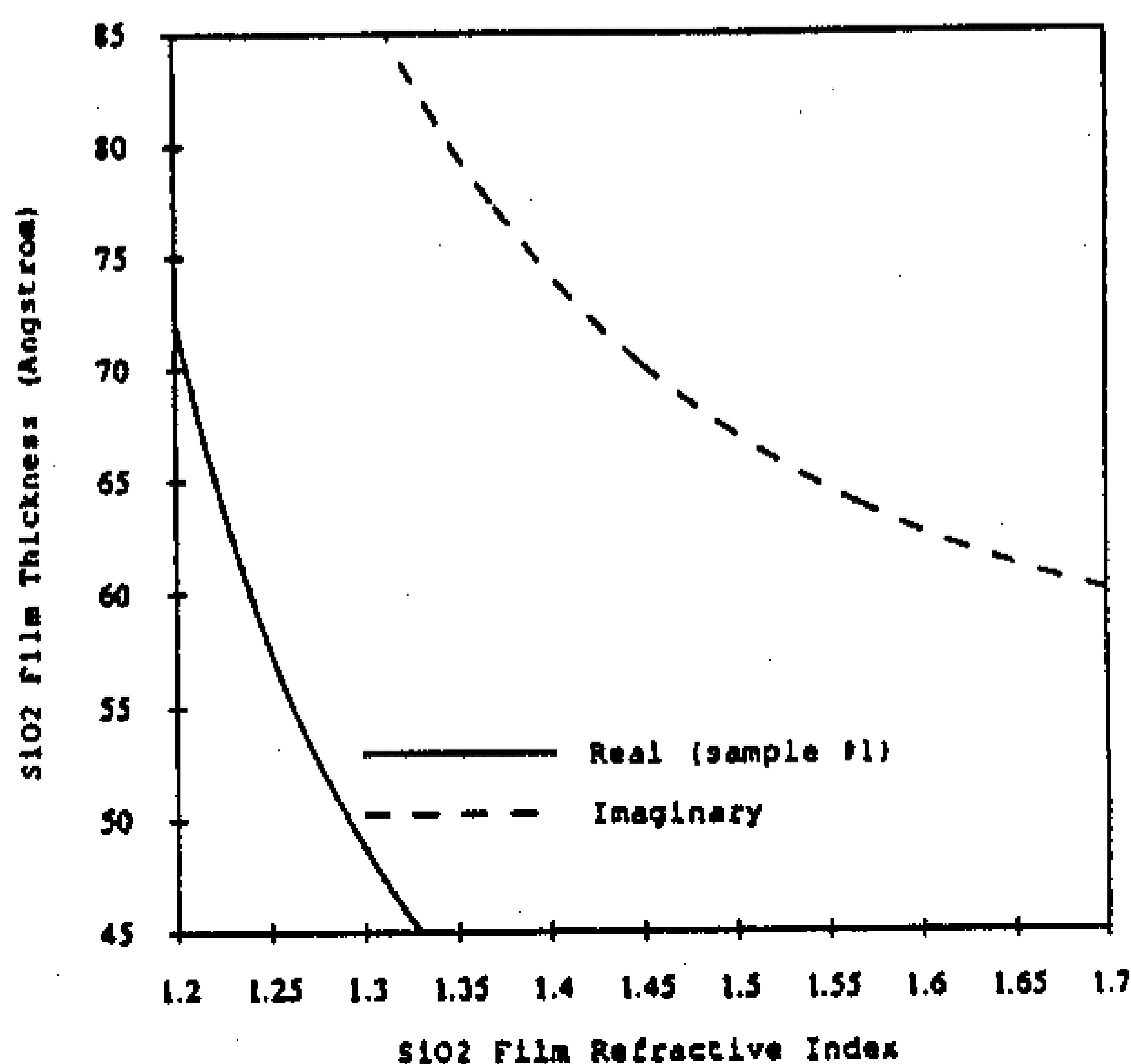

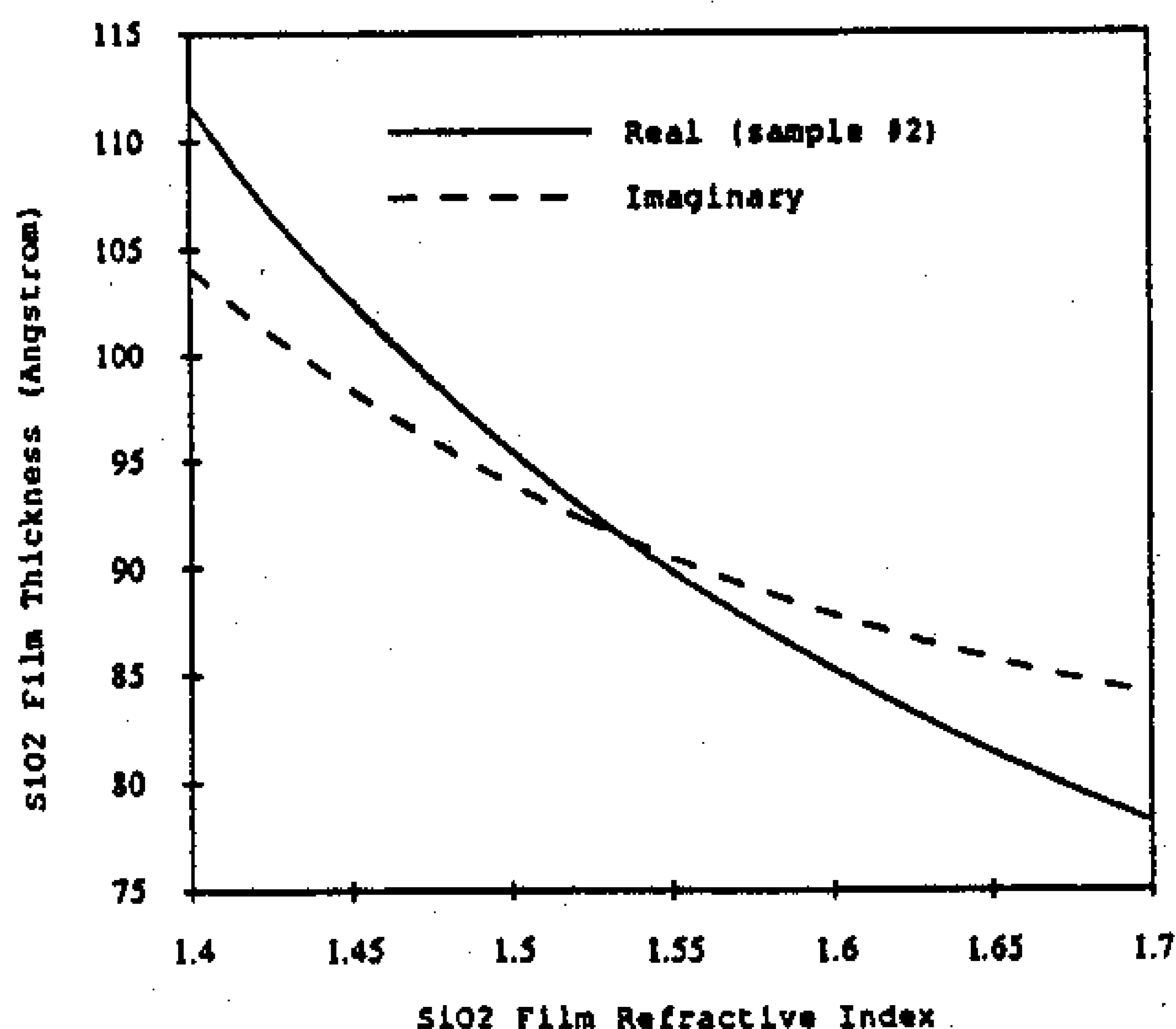

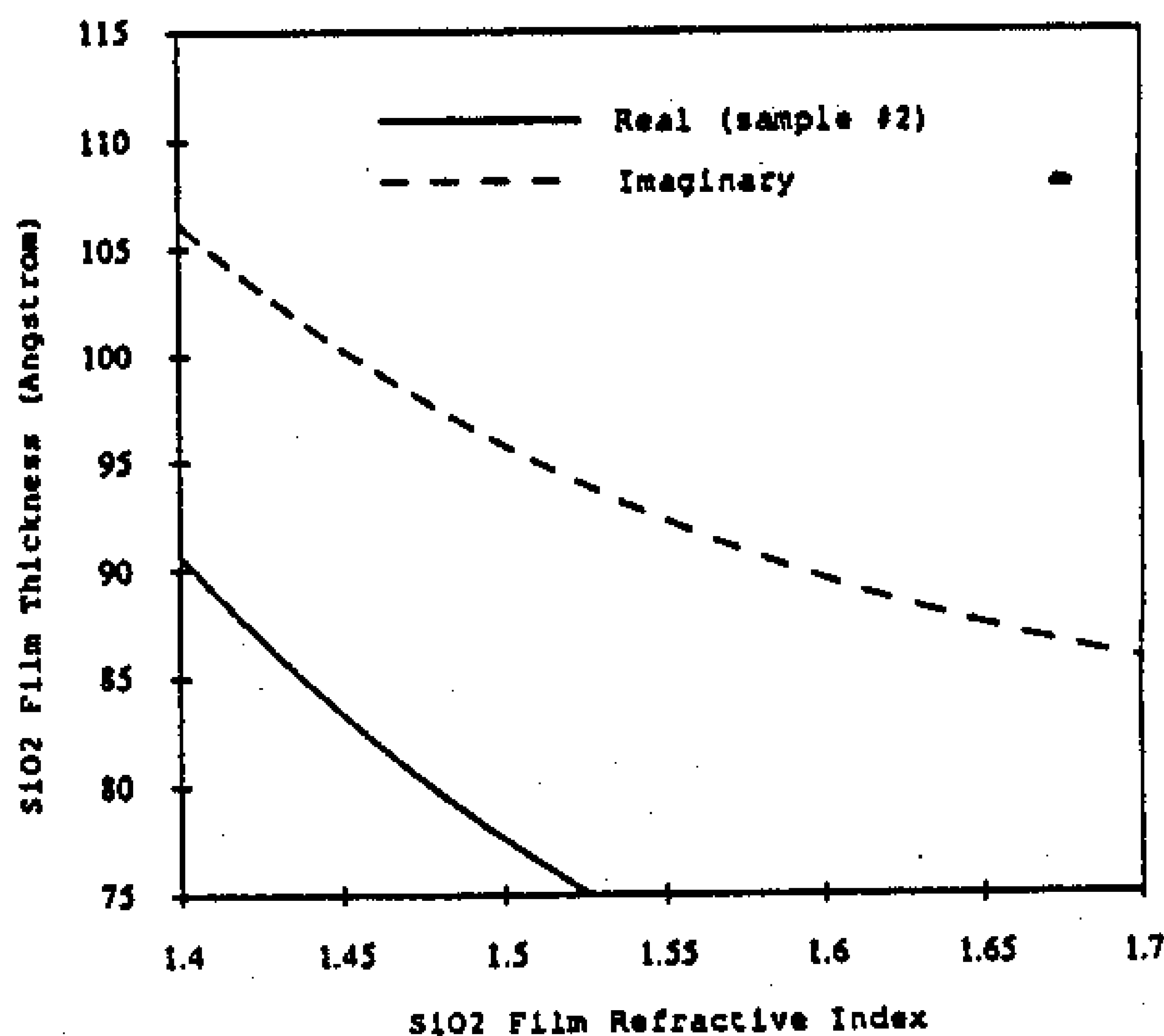

Fig. 3. Hardware-dependent ellipsometric data acquisitions and reductions. (a, top left) Δ = 160.089°, ψ = 10.910°, AOI = 70.011°, measured by Rudolph 436. (b, top right) Δ = 160.01°, ψ = 11.11°, AOI = 70.0°, measured by Gaertner L104SA. (c, bottom left) Δ = 152.429°, ψ = 11.337°, AOI = 70.012°, measured by Rudolph 436. (d, bottom right) Δ = 152.35°, ψ = 11.52°, AOI = 70.0°, measured by Gaertner L104SA.

Table III. Calculated Δ and ψ values from hypothetical bulk and interfacial film thicknesses (d_1, d_2) and their respectable refractive indexes ($n_1 = 1.46$, $n_2 = 2.8$) of the two-layer model with AOI = 70°, WVL = 6328 Å, (100) silicon substrate with n-Si = 3.8737 and k-Si = 0.018, n-air = 1.0003, using the algorithm of this study with double precision FORTRAN and the algorithm of Irene's research group (7)

Table IIIa. Calculated Δ and ψ values and solutions of bulk film thickness ($d_{1,s}$) and refractive index ($n_{1,s}$) using the algorithm of this study (using untruncated Δ and ψ data).

d_1 (Å)	d_2 (Å)	Δ	ψ	$d_{1,s}$ (Å)	$n_{1,s}$
50	8	163.0207043	10.8124439	50.00000	1.4599999
100	10	149.5888608	11.5578524	100.00000	1.4600000
150	12	137.9234377	12.6453882	149.99996	1.4600000
1000	14	79.1655297	41.6707657	999.99994	1.4600000

Table IIIb. Calculated Δ and ψ values and solutions of bulk film thickness ($d_{1,s}$) and refractive index ($n_{1,s}$) using the algorithm of Irene's research group.

d_1 (Å)	d_2 (Å)	Δ	ψ	$d_{1,s}$ (Å)	$n_{1,s}$
50	8	163.0207098	10.8124457	50.0009	1.45998
100	10	149.5888681	11.5578540	100.0002	1.46000
150	12	137.9234459	12.6453896	150.0003	1.46000
1000	14	79.1655346	41.6707655	999.9998	1.46000

and an optional graph such as that shown in Fig. 2. In order to evaluate whether the mathematical structure of the ellipsometry equation is coded correctly in the proposed algorithm, the following software comparison with established ellipsometric data reduction algorithms was conducted.

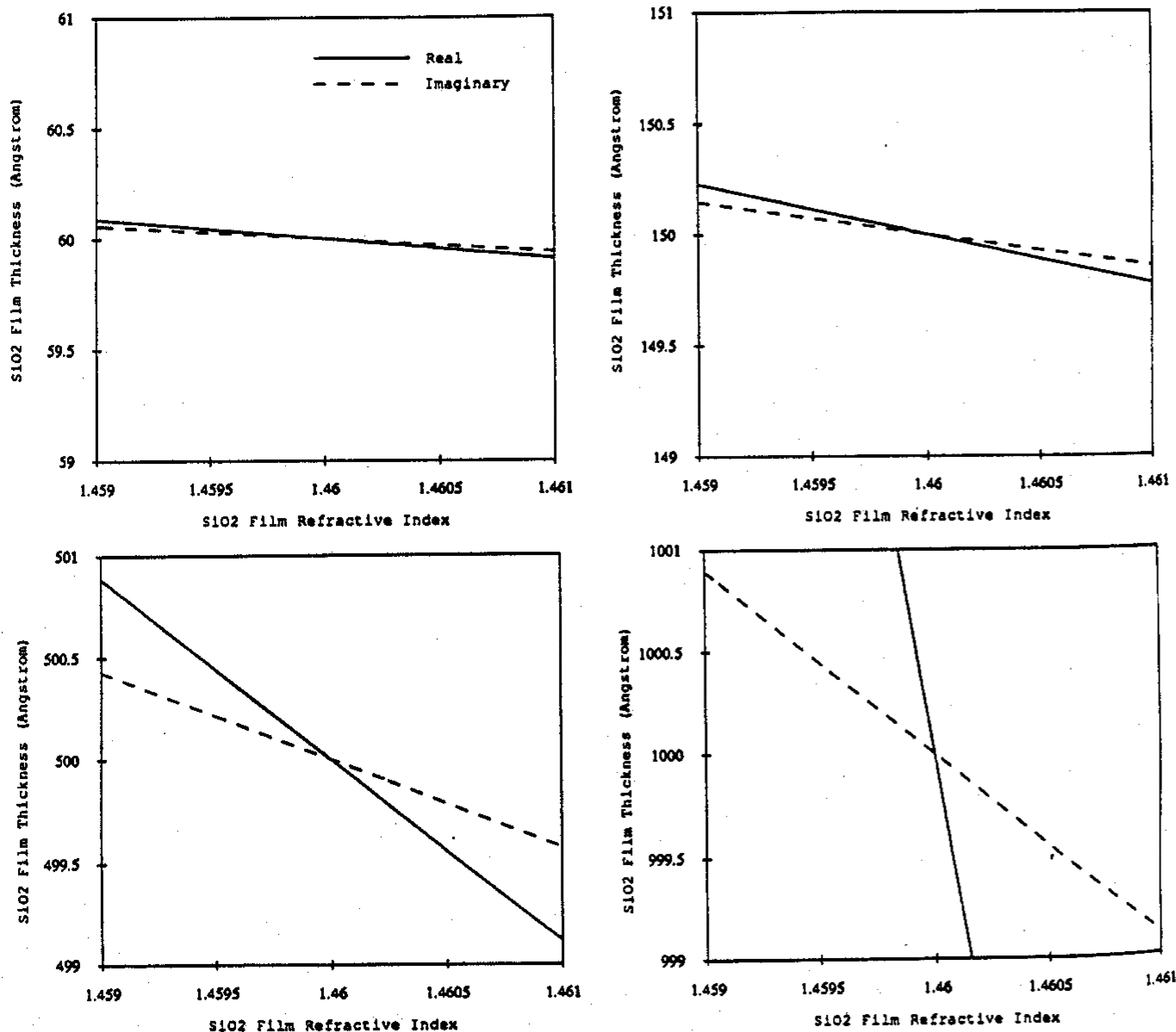

Fig. 4. Ellipsometric real and imaginary curves on thickness vs. refractive index plane. (a, top left) Film with $n = 1.46$, thickness 60 Å. (b, top right) Film with $n = 1.46$, thickness 150 Å. (c, bottom left) Film with $n = 1.46$, thickness 500 Å. (d, bottom right) Film with $n = 1.46$, thickness 1000 Å.

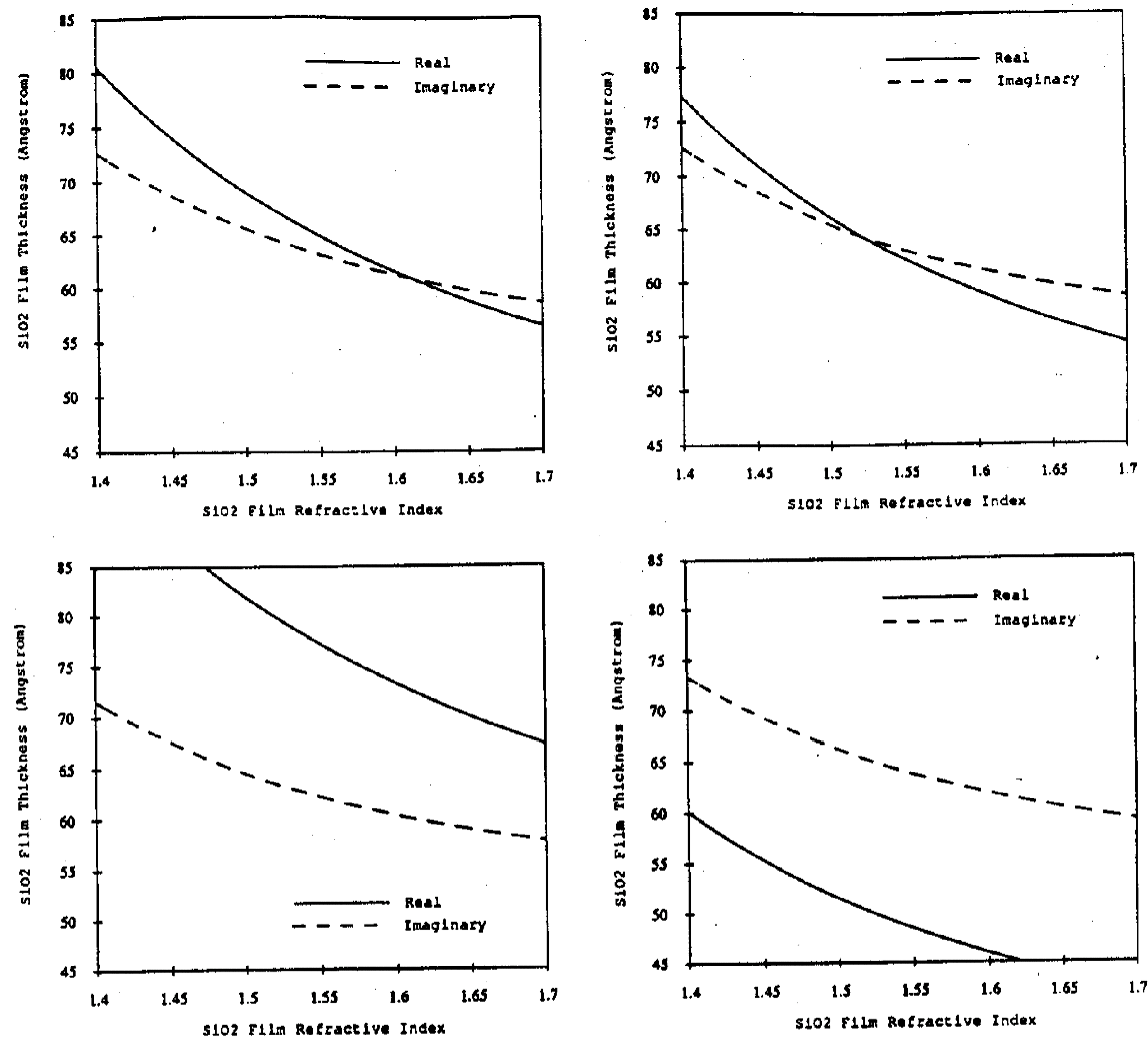

Fig. 5. Error-induced drifts of ellipsometry real and imaginary curves on thickness vs. refractive index plan. (a, top left) Original solution graph of sample No. 1, Δ, and ψ measured by Rudolph 436, assuming Δ-error = 0°, ψ-error = 0°, AOI-error = 0°. (b, top right) Assuming Δ-error = 0°, ψ-error = 0°, AOI-error = 0.01° (c, bottom left) Assuming Δ-error = 0.1°, ψ-error = − 0.1°, AOI-error = 0°. (d, bottom right) Assuming Δ-error = 0°, ψ-error = 0.1°, AOI-error = 0°.

First, Δ and ψ were calculated from eight sets of hypothetical films/substrate structures, with film thickness ranging from 40 Å to 1000 Å. Equation [1] was used to determine Δ and ψ, using a one-layer model, as shown in Table I. These hypothetical Δ and ψ were then fed into both the software developed in this study, and that associated with the Gaertner Scientific Ellipsometer L104SA. Table II shows the computed refractive index and film thickness results using the algorithm of this study and that of the Gaertner L104SA. Refractive index results are rounded off to the third decimal place and thickness results are rounded off to the nearest angstrom. Truncation of Δ and ψ data to the third decimal place mimics the limitation of research grade ellipsometers, with polarizer and analyzer resolutions of 0.01° (the third decimal place can be estimated, for instance, from the scale reading on the Rudolph 436 ellipsometer).

Based on the results of Table II, it is likely that the two algorithms are equally reliable since both yield similar answers to the specified precision (three digits following the decimal). Compared with the thicknesses and indexes of the hypothetical films of Table I, it is also concluded the error of the computed index for thin oxides (in this case less than 70 Å) is due to Δ and ψ data truncation error, and not the software algorithm employed. Note that ensuring the precision of measured refractive index down to the third digit after the decimal is beyond the usual research grade ellipsometer with a resolution of 0.01°, for SiO_2 films thinner than 70 Å.

Another comparison with the algorithm (7) using Eq. [1] and a two-layer model, is shown in Table III. In this case, the hypothetical film/substrate structure is a bulk film ($n_1 = 1.46$, thickness d_1) and an interfacial film ($n_2 = 2.8$, thickness d_2) on silicon. Again, the agreement of computed results between the two algorithms is excellent. We thus infer the mathematical structure of the proposed algorithm was implemented correctly.

The following experiment using different hardware clearly demonstrates the importance of accurate, raw Δ and ψ acquisition in ellipsometric data reduction. The Rudolph Research Model 436 manual ellipsometer and the Gaertner Scientific Ellipsometer L104SA are both used to measure two samples (No. 1 and No. 2)[1].

[1] This work only intends to compare ellipsometers with different resolutions, not different manufacturers. In fact, both Gaertner and Rudolph make research grade ellipsometers with resolution of 0.01°.

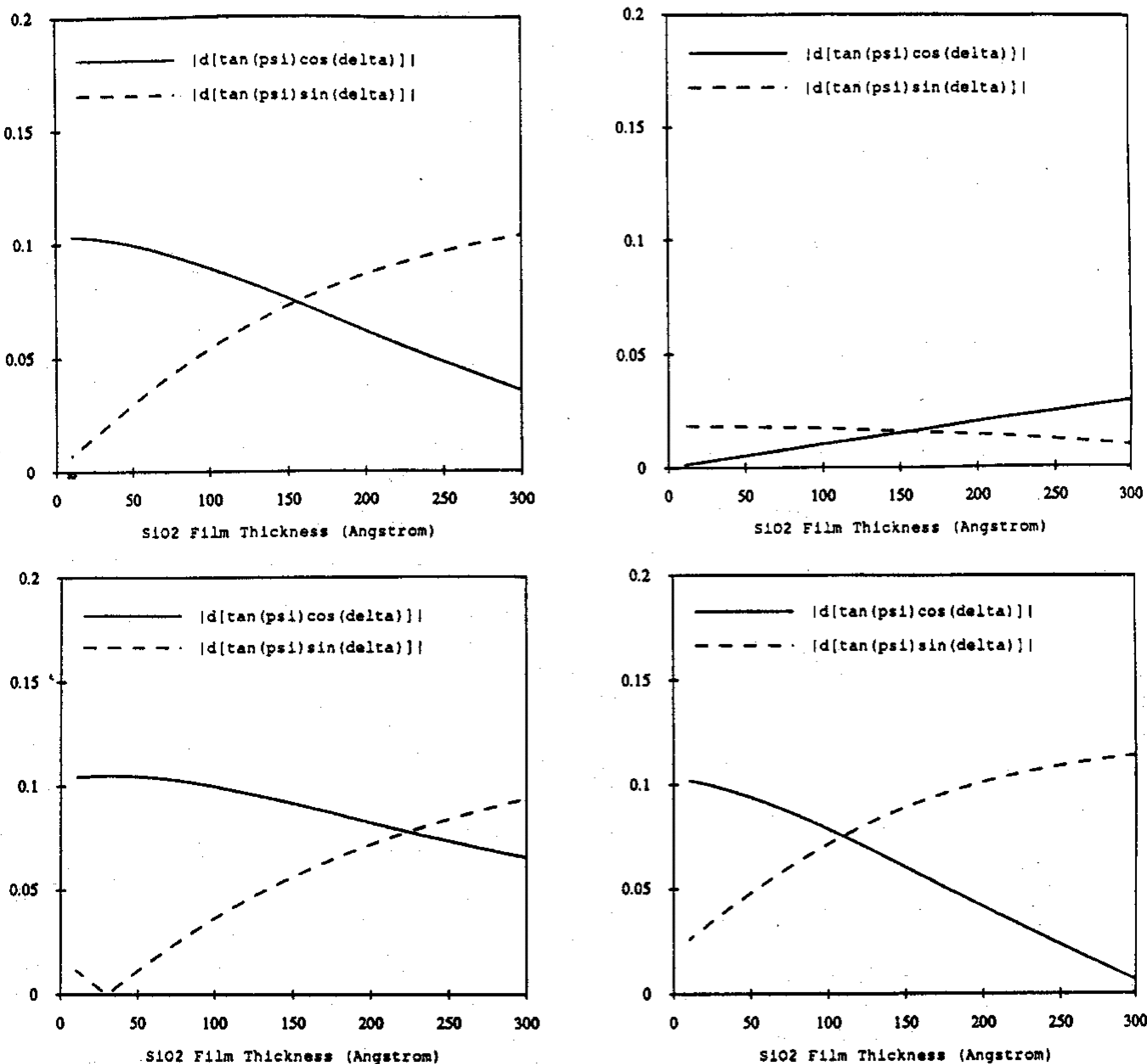

Fig. 6. Sensitivity to measurement-error of ellipsometric real and imaginary parts as a function of film thickness. (a, top left) $d\Delta = 0.1°$, $d\psi = 0°$ (b, top right) $d\Delta = 0°$, $d\psi = 0.1°$ (c, bottom left) $d\Delta = 0.1°$, $d\psi = 0.1°$ (d, bottom right) $d\Delta = 0.1°$, $d\psi = -0.1°$.

Figures 3b and d show the case studies for which the Gaertner program yields "NO ANSWER" for thin oxide Δ and ψ inputs measured with a Gaertner L1045A. This may mean either the iterating routine of the Gaertner program failed to converge, or the solution is outside the physical region. The same situation may well apply to other commercial ellipsometry software. However, the Δ, ψ, and AOI data obtained by the manual ellipsometer were then fed into the Gaertner program and the program gave exactly the same answer (film thickness rounded to the nearest angstrom and refractive index rounded to the third decimal place) as obtained with the algorithm of this study. This is shown in Fig. 3a and c. Thus the difficulty encountered in obtaining thickness and index simultaneously for thin SiO_2 films is due to the measurement hardware resolution, rather than software reliability.

Some Intrinsic Properties of the Ellipsometry Equation Revealed by the Graphical Data Reduction Algorithm, and Their Implications

From the solution graphs which monitor the ellipsometric data reduction process for various SiO_2 film/substrate structures, a few unique properties of the ellipsometry equation are revealed. These properties were not found previously with other ellipsometric data reduction algorithms.

Figure 4 shows four simulated thickness and refractive index solution graphs with a progressive increase of SiO_2 film thickness. The difference in slopes between the real and imaginary parts of the ellipsometry equation decreases as the film thickness approaches zero. The same trend is observed for thicknesses greater than ~1400 Å, increasing towards the first ellipsometric cycle thickness. The difficulty in obtaining accurate curve intersection increases as film thickness approaches the ellipsometric cycle thickness, since the two curves begin to merge together. Both real and imaginary curves must be positioned with great precision on the two-unknown plane for thin SiO_2 films. Following the projected trend in Fig. 4, the two curves will be superimposed as the film thickness approaches zero, just as the isoindex curves converge to the zero thickness point in a conventional nomogram.

The importance of accurate ellipsometric measurements grows larger for very thin films (*e.g.*, less than 200 Å) (8, 9). Figure 5 simulates the impact of measurement error on ellipsometric data reduction for sample No. 1 (ellipsometric data has been measured by the manual, research grade ellipsometer for this example). A 0.1° measurement error in Δ and ψ, or 0.01° error of AOI, is enough to drift the solution away from the original one of Fig. 5, for which no measurement error is assumed. Note that most automatic rotating analyzer ellipsometers have polarizer and ana-

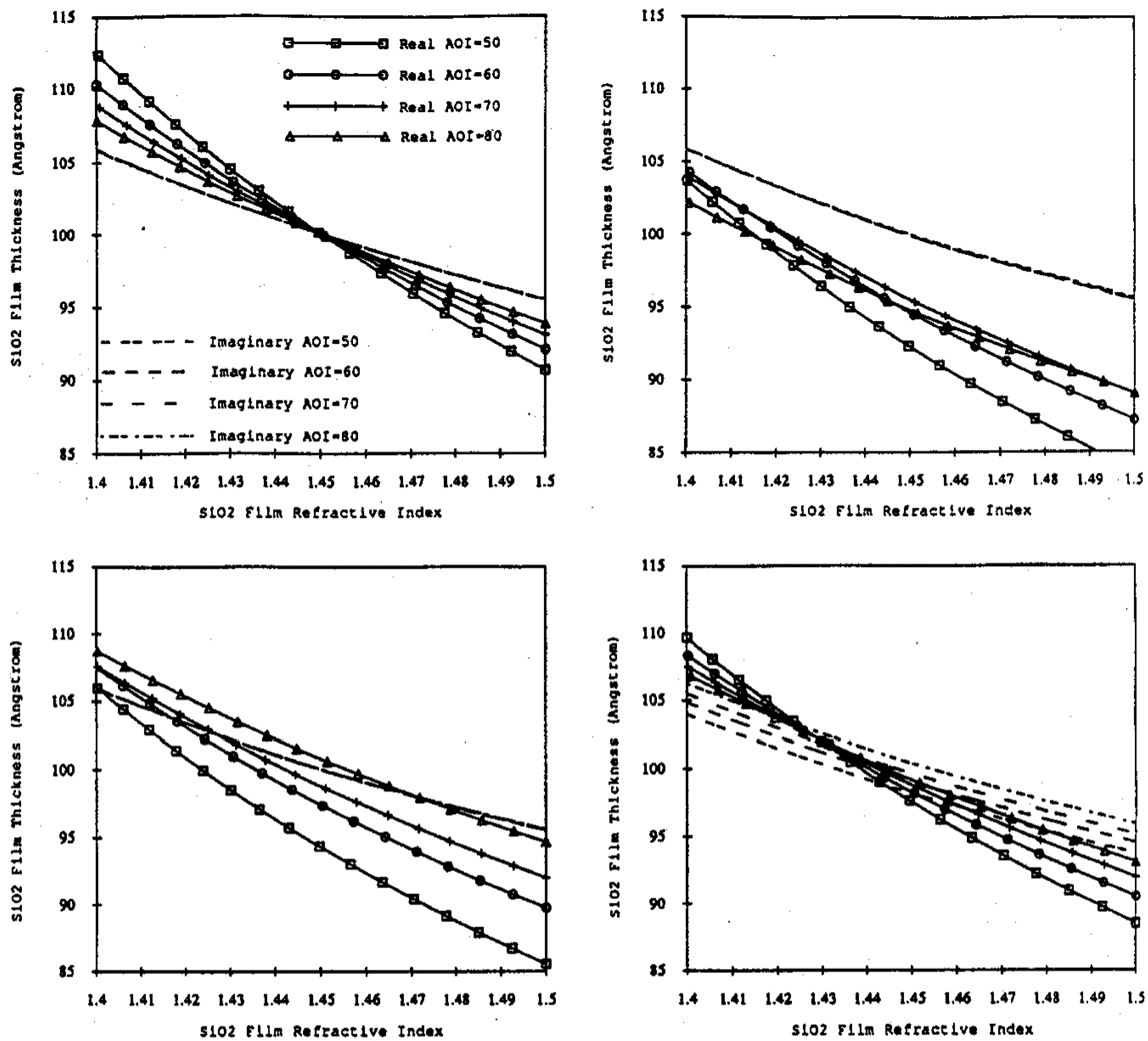

Fig. 7. Impact of measurement errors on multiple-angle-of-incidence ellipsometry. (a, top left) Original solution graph of 100 Å thick SiO_2 on Si with n-SiO_2 = 1.45, assuming Δ-error = 0°, ψ-error = 0°, AOI-error = 0°. (b, top right) Assuming Δ-error = 0°, ψ-error = 0°, AOI-error = 0.02°. (c, bottom left) Assuming Δ-error = 0°, ψ-error = 0.01°, AOI-error = 0°. (d, bottom right) Assuming Δ-error = 0.1°, ψ-error = 0°, AOI-error = 0°.

lyzer resolutions of around 0.1°, limited by the precision of the stepping motor. Similar sensitivity of the solution (curve intersection) to measurement error has also been observed for other Δ, ψ, and AOI error combinations for thin oxides (less than 300 Å) in this work. However, the imaginary part of the ellipsometry equation has always been found numerically to have an impressive resistance to measurement errors as shown in Fig. 5.

A total differential expression is used to evaluate the sensitivity of real and imaginary parts of Eq. [1] to Δ- and ψ-measurement-error. The total differential expression for both the real and imaginary parts is as follows

Real:

$$d[\tan(\psi)\cos(\Delta)] = \cos(\Delta)\sec^2(\psi)d\psi - \sin(\Delta)\tan(\psi)d\Delta \quad [8]$$

Imaginary:

$$d[\tan(\psi)\sin(\Delta)] = \sin(\Delta)\sec^2(\psi)d\psi + \cos(\Delta)\tan(\psi)d\Delta \quad [9]$$

A series of plots of these expressions *vs.* film thickness for all possible combinations of $d\Delta$ and $d\psi$ are shown in Fig. 6 (AOI = 70°, n-SiO_2 = 1.61, wave length (WVI) = 6328 Å, SiO_2 film on Si). Though it is generally true for oxides thinner than 100 Å that the imaginary part is less sensitive than the real part to Δ and ψ errors, Figure 6b predicts the imaginary part is more ψ-measurement-error sensitive. This contradicts the actual situation of Fig. 5d. The complexity of the real and imaginary curves' sensitivity to Δ- and ψ-measurement-error thus lies beyond a simple analysis.

Nevertheless, for the situation where it is necessary to fix refractive index to obtain the thin-film thickness due to either poor ellipsometric data measurement or poor convergence of the iterating data reduction algorithm, the imaginary part of the ellipsometry equation should be used, based on its impressive resistance to measurement-error-induced variation in computed refractive index and film thickness. A data reduction algorithm using both the real and imaginary curves of the ellipsometry equation will experience solution accuracy degradation, as indicated in Fig. 5c and d, the solution (intersection of real and imaginary curves) is outside the physically meaningful region. Once this does happen, the commercial ellipsometry program usually says "NO ANSWER."

A multiple AOI ellipsometric simulation in Fig. 7a, using 100 Å thick SiO_2 film on Si with n-SiO_2 = 1.45, indicates the imaginary part of the ellipsometry equation is almost AOI-

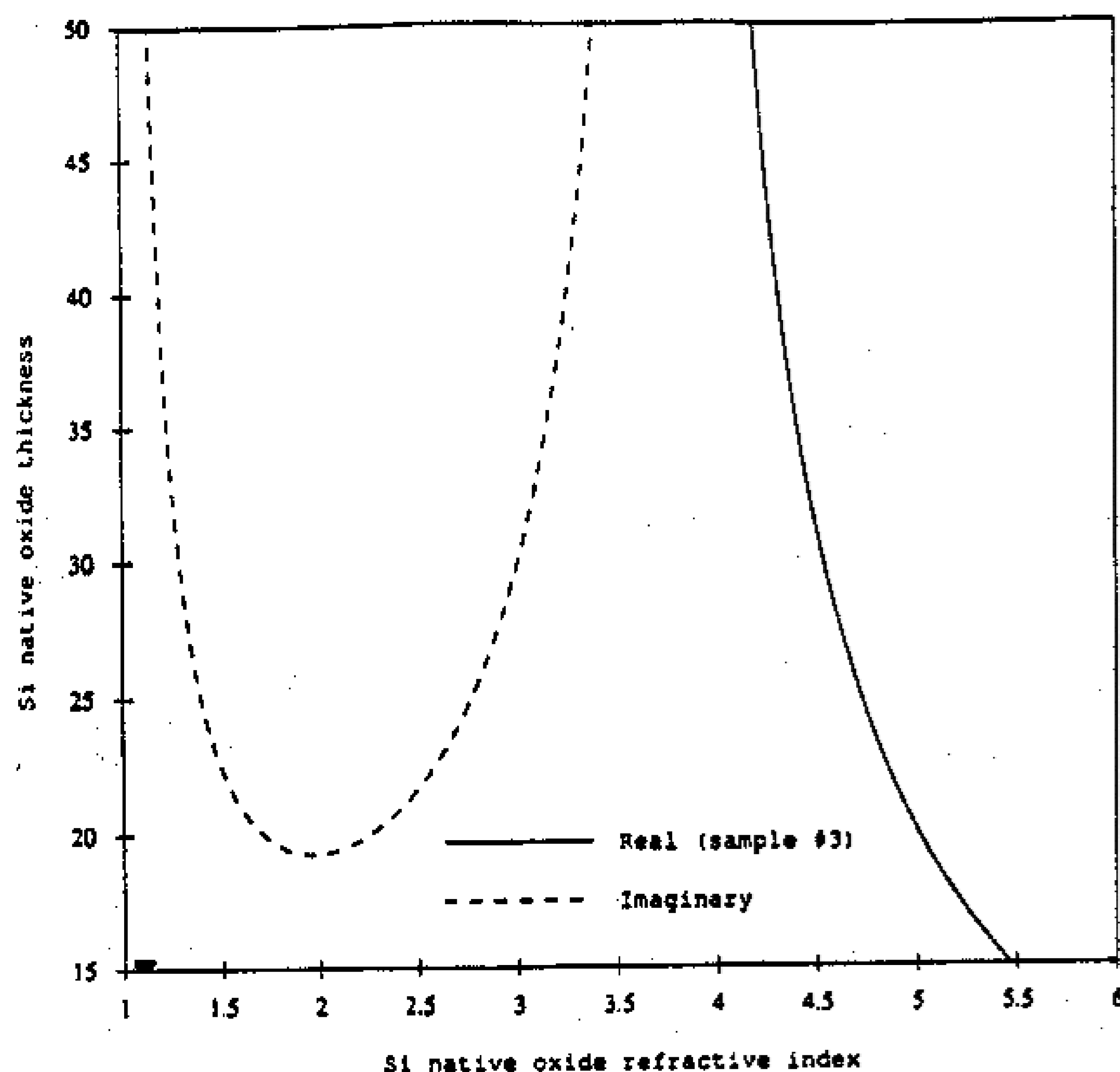

Fig. 8. Ellipsometric data reduction for Si native oxide (sample No. 3). $\Delta = 172.69°$, $\psi = 10.73°$, AOI = 70°, measured with Gaertner L1045A.

independent for thin oxides. Thus, measurement errors in AOI drift only the real part as shown in Fig. 7b. The imaginary part is not only ψ-measurement-error insensitive for AOI ranging from 50 to 80° shown in Fig. 7c, but also Δ-measurement-error insensitive for AOI ranging from 70 to 80° shown in Fig. 7d. However, the imaginary part of the ellipsometry equation is highly AOI-dependent for a 1000 Å thick SiO_2 film on Si with n-SiO_2 = 1.45.

An example of using the proposed algorithm to offer solution compensation in ellipsometric data reduction is given in Fig. 8. The Gaertner ellipsometric program yields "NO ANSWER" in solving film thickness and index simultaneously for sample No. 3 (Si native oxide) using the ellipsometric data obtained with the Gaertner ellipsometer L104SA. The same ellipsometric data measured with a Gaertner L1045A ($\Delta = 172.69°$, $\psi = 10.73$ at AOI = 70°) was fed into our program and it gave a solution graph shown in Fig. 8. Obviously the solution (intersection of the real and imaginary curves) is outside the physical region which explains the "NO ANSWER" result given by the Gaertner program. However, since the imaginary part of the ellipsometry equation has an impressive resistance to ellipsometric measurement errors in measuring thin SiO_2 films on Si at wavelength 6328 Å, it can be concluded from the imaginary curve in Fig. 8 that the native oxide thickness is around 20 Å, since it is not unreasonable to assume that the index of refraction of native oxide is in the range of 1.45 to 2.5.

The phenomena represented through Fig. 4-7 were also observed in a nonabsorbing, two-layer model; specifically, a 100 Å bulk film and an interfacial layer of SiO_x (n-SiO_x = 2.8, d-SiO_x = 10 Å, $x < 2$) on silicon.

The special case of an absorbing, one-layer film is also examined. A set of multiple AOI ellipsometric simulations similar to that in Fig. 7 (using 100 Å silicon nitride (noncrystalline) on a Si substrate with n-Si_3N_4 = 2.278, k-Si_3N_4 = 4.9×10^{-3}, n-Si = 1.57, k-Si = 3.565 at wavelength of 2480 Å (5 eV) (10) indicates both the real and imaginary parts of the ellipsometry equation are highly AOI-dependent, and so appear to have equal sensitivity to ellipsometric measurement errors.

Summary and Conclusions

A graphical ellipsometric data reduction algorithm, based on tracing both the real and imaginary parts of the ellipsometry equation, was fully described. The mathematical structure of the proposed algorithm was implemented and tested by comparing numerical results of both one- and two-layer models with other established algorithms. Using the graphical ellipsometric data reduction algorithm, it was found in thin SiO_2 film (on silicon) ellipsometric measurement using both one- and two-layer models:

1. difficulties encountered in obtaining thickness and index simultaneously are attributable to measurement hardware resolution, rather than the reliability of software associated with the hardware;
2. the imaginary part of the ellipsometry equation is almost AOI-independent;
3. the imaginary part is not only ψ-measurement-error insensitive for AOI ranging from 50 to 80°, but also Δ-measurement-error insensitive for AOI ranging from 70 to 80°.

Thus whenever it is necessary to fix refractive index to obtain thin SiO_2 film thickness from the ellipsometry equation, using either one- or two-layer film models, only the imaginary part of the ellipsometry equation should be used, based on its resistance to measurement errors, to offer compensation to the final solution of film thickness. This conclusion is based on numerical simulations of error sensitivity.

The advantages of the proposed algorithm over other ellipsometric data reduction algorithms are: the ability to monitor the extraction process for finding the unknowns; the ability to pinpoint the source of measurement problems, the ability to simulate the impact of measurement error on data reduction, and the ability to compensate the final solutions to correct for these errors in the Si-SiO_2 system.

Acknowledgments

The authors thank Dick Baker of IBM GTD Essex Junction for wafer oxidation preparations, Jack Rogers of IBM GTD Essex Junction for assistance in the manual ellipsometer experiment, and Professor E. A. Irene of University of North Carolina for arranging the ellipsometric software comparison. This work was supported by an IBM-Shared University Research Grant through IBM GTD Essex Junction.

Manuscript submitted Oct. 28, 1991; revised manuscript received Jan. 29, 1992.

Thayer School of Engineering assisted in meeting the publication costs of this article.

REFERENCES

1. A. Kalnitsky, S. P. Tay, and I. D. Calder, *This Journal*, **135**, 1271 (1988).
2. J. C. Panner, E. W. Conrad, and J. L. Rogers, *Thin Solid Films*, **206**, 381 (1991).
3. G. A. Candela, D. Chandler-Horowitz, J. F. Marchiando, D. B. Novotny, B. J. Belzer, and M. C. Croarkin, NIST Special Publication 260-109, U.S. Government Printing Office, Washington, DC (Oct. 1988).
4. R. M. A. Azzam and N. M. Bashara, "Ellipsometry and Polarized Light," North-Holland Pub. Co., Amsterdam (1977).
5. A. Daude, A. Savary, A. Seignac, and S. Robin, *Optica Acta*, **20**, 353 (1973).
6. W. R. Hunter, *J. Opt. Soc. Am.*, **55**, 1197 (1965).
7. Private communications with E. A. Irene. The algorithm is described in S. Chongsawangvirod, E. A. Irene, A. Kalnitsky, S. P. Tay, and J. P. Ellul, *This Journal*, **137**, 3536 (1990).
8. J. H. Ho, C. L. Lee, C. W. Jen, and T. F. Lei, *Solid-State Electron.*, **330**, 973 (1987).
9. A. Kalnitsky, S. P. Tay, J. P. Ellul, S. Chongsawangvirod, J. W. Andrews, and E. A. Irene, *This Journal*, **137**, 234 (1990).
10. H. R. Philipp, in "Handbook of Optical Constants of Solids," E. D. Palik, Editor, p. 774, Academic Press, Inc. (1985).